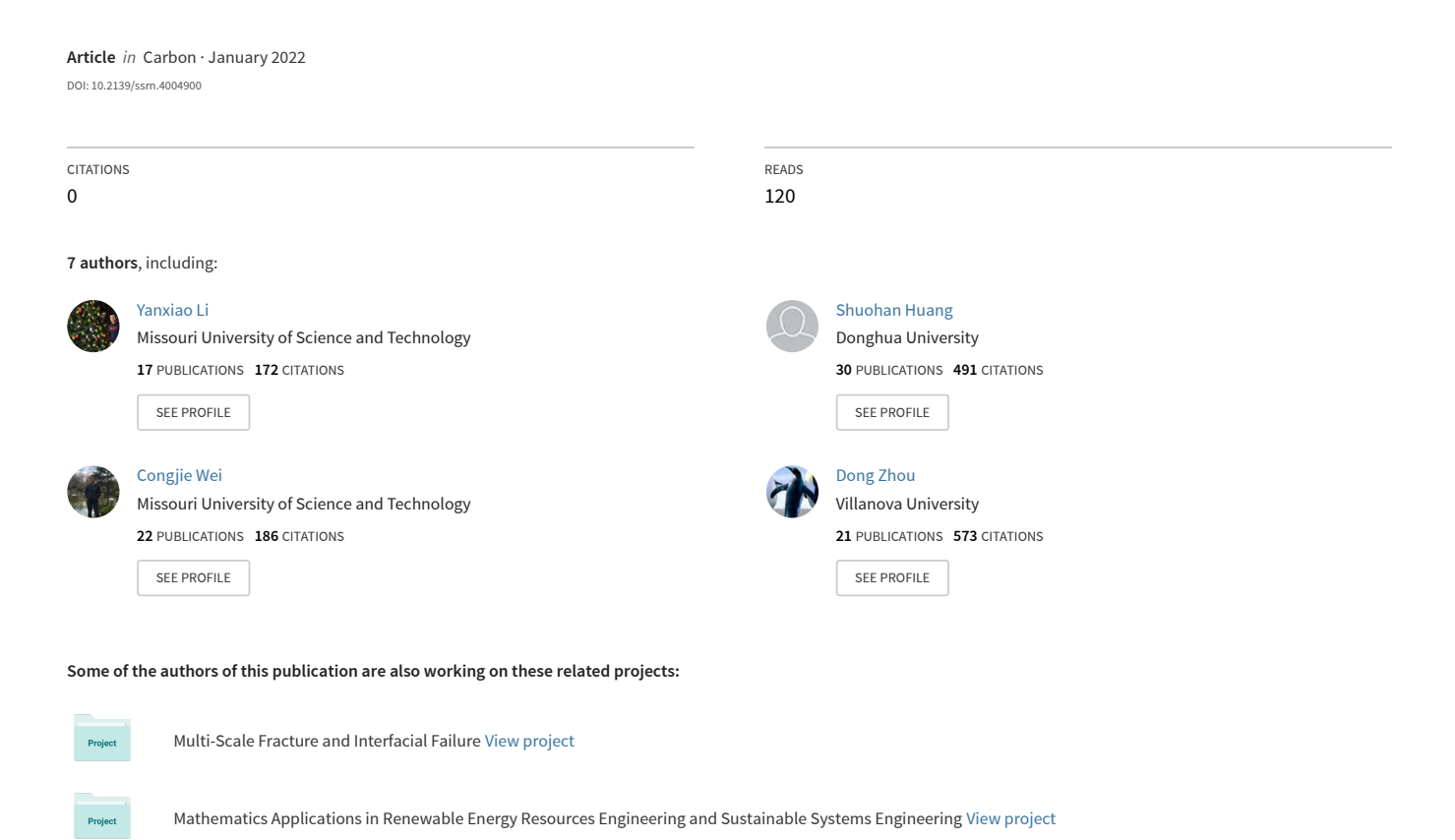
Friction between Mxenes and Other Two-Dimensional Materials at the Nanoscale



Friction Between MXenes and Other Two-Dimensional Materials at the Nanoscale

Yanxiao Li¹, Shuohan Huang^{2,3†}, Congjie Wei¹, Dong Zhou⁴, Bo Li⁴, Vadym N. Mochalin^{2,5*} (http://orcid.org/0000-0001-7403-1043), Chenglin Wu^{1,5,6*} (http://orcid.org/0000-0001-7733-1084),

¹Department of Civil, Architectural, and Environmental Engineering, Missouri University of Science and Technology, Rolla, MO 65401, USA

²Department of Chemistry, Missouri University of Science and Technology, Rolla, MO 65401,

USA

³State Key Laboratory for Modification of Chemical Fibers and Polymer Materials, College of Materials Science and Engineering, Donghua University, Shanghai 201620, China
 ⁴Department of Mechanical Engineering, Villanova University, Villanova, PA 19085, USA
 ⁵Department of Materials Science and Engineering, Missouri University of Science and Technology, Rolla, MO 65409, USA

⁶Department of Chemical and Biochemical Engineering, Missouri University of Science and Technology, Rolla, MO 65409, USA

[†]This author contributes equally to the first author

*Corresponding author E-mail: wuch@mst.edu, mochalinv@mst.edu

^{*}Corresponding author. Tel: 573 341-4465. Email: wuch@mst.edu (Chenglin Wu)

^{*}Corresponding author. Tel: 573 341-6043. Email: mochalinv@mst.edu (Vadym N. Mochalin)

Abstract

Two-dimensional (2D) materials have unique friction properties that are different from their 3D

counterparts. MXenes, a large family of 2D transition metal carbides, carbonitrides, and nitrides,

have recently attracted attention as solid lubricants on the macroscale. Here we experimentally

investigate the friction of Ti₃C₂T_x and Ti₂CT_x MXenes against Ti₃C₂T_x and Ti₂CT_x MXenes,

graphene, and MoSe₂ at the nanoscale, using atomic force microscopy (AFM). Ti₃C₂T_x and Ti₂CT_x

MXene coated SiO₂ spherical AFM probes were used to slide against films of these materials with

varying number of monolayers deposited on the substrate. We have found that over the 15 nm

sliding distance the measured nanoscale coefficients of friction (COFs) for all the investigated 2D

interfaces are below 0.01. At the same time, hydrogen bonding involving -O- and -OH surface

terminating groups on MXenes induced higher friction forces for the MXene/MXene contacts

compared to other contacts. Moreover, a less significant number-of-monolayers effect on the

friction was observed for MXenes due to their thicker monolayers compared with other 2D

materials in this study. These results further contribute to our understanding of the mechanisms of

friction of MXenes and reveal the potential of MXenes as tunable lubricants at the nanoscale.

Keywords: MXenes; 2D materials; Friction; Nanoscale

1. Introduction

MXenes, a large family of two-dimensional (2D) materials, are commonly synthesized by removing A element layers from MAX phases with HF etching in aqueous environment. MAX phases are bulk ternary carbides, carbonitrides or nitrides with the general formula $M_{n+1}AX_n$, where M is an early transition metal, A is an A-group element (mostly group IIIA or IVA), X is either carbon or nitrogen, and an integer n is within 1-4 [1-3]. During selective etching of MAX phases in aqueous environment, the resulting exfoliated MXene layers are always terminated with -F, -OH, and/or -O- groups. Thus, MXenes are referred to as $M_{n+1}X_nT_x$, where T represents the surface terminations (-F, -OH, and/or -O-) and x is the (unknown) fraction of T per formula unit. Around 30 different MXenes have been synthesized [4, 5] and more are expected to be exfoliated from >70 reported MAX phases in the future [6-8]. MXenes have shown attractive electronic, optical and magnetic properties [9-13], great potential in sensing [14-16], energy harvesting [17] and storage [4, 18], as well as electromagnetic shielding applications [19-23]. In prior research we have shown a higher adhesion energy at MXene/MXene interfaces than between MXene and other 2D materials, including graphene and MoSe₂ [24]. MXene frictional properties are also critically important for applications in solid lubricant coatings [25, 26], triboelectric nanogenerators [17], and wearable electronics [27, 28]. However, not many studies in the emerging area of MXene tribology have been published so far [25, 29-33].

One- to a few atoms-thick, 2D materials have unique friction and wear properties that are different from their 3D counterparts [34-37]. Atomic force microscopy (AFM) friction experiments on interfaces between SiO₂ and a group of 2D materials including graphene, graphene oxide, MoS₂, NbSe₂, and h-BN have shown that measured coefficients of friction (COFs), depend on both the surface conditions (including roughness [38], and surface terminations [39]) and the contact-

induced elastic deformation, which is a function of bending rigidity of the 2D materials [40-42]. Bending rigidity of MXenes has been calculated to be higher than one-atomic layer thick 2D materials [43]. Due to their tunable monolayer thickness, achieved by changing n in M_{n+1}X_nT_x, and rich surface chemistry with a large number of terminating groups, MXene frictional properties were suspected to differ from other 2D materials based on computational investigations [44]. However, most experiments so far were limited to MXene friction against bulk materials. Ball-on-disc friction experiments with delaminated MXenes using a 9.526 mm diameter diamond-

like carbon (DLC) coated steel ball have demonstrated that Ti₃C₂T_x MXene is superlubric (COF <0.01 against DLC) under dry nitrogen environment [29]. Similar experiments with multilayered MXene and 6 mm diameter Al₂O₃ balls revealed surface terminations and intercalated water as key parameters influencing the frictional performance of Ti₃C₂T_x nanoparticles [30]. Experiments with Ti₃C₂T_x and 3.969 or 10 mm diameter 100Cr6 steel balls carried out under different normal pressures and humidity levels showed a significant reduction in friction under 0.8 GPa load and lower relative humidity of 20% [25]. Few-layer Ti₃C₂T_x nano-sheets were also reported as solid lubricants on SiO₂ substrates, with inferior friction mitigation capabilities compared with graphene and MoS₂ in AFM experiments [45].

At the nanoscale, AFM experiments with a 20 nm diameter silicon nitride probe were conducted to investigate the effects of surface terminations on the friction of Ti₃C₂ MXene [31]. The measured COF ranged from 0.007 to 0.01, indicating possible superlubricity of Ti₃C₂ produced by etching with LiF and HCl. AFM experiments with a 160 nm diameter SiO₂ probe found that a lower normal pressure and oxidation of Ti₃C₂T_x surface reduced the friction [32]. Similar experiments with Ti₃C₂ and Nb₂C MXenes showed that friction is related to dipole moment of the material [33].

Experiments mentioned above have demonstrated exceptionally low friction of MXenes against bulk materials (DLC, Al₂O₃, 100Cr6 steel, SiO₂, Si₃N₄). However, with much higher deformability of 2D materials compared to bulk ones, and higher adhesion measured between MXenes and other 2D materials, it is not certain whether the low friction of MXenes against bulk materials will stay unchanged when MXenes are sled against other 2D materials.

In this paper, we experimentally investigate the nanoscale friction of $Ti_3C_2T_x$ and Ti_2CT_x MXenes against the MXenes, as well as against graphene and MoSe₂. We measured friction forces by sliding the bare, as well as $Ti_3C_2T_x$ and Ti_2CT_x coated, SiO_2 spherical AFM probes against graphene, MoSe₂, $Ti_3C_2T_x$, and Ti_2CT_x films with varying number (1-25) of the MXene monolayers and normal forces (0-2 μ N). We have found that the nanoscale (15 nm sliding distance) COFs for all the investigated 2D interfaces are below 0.01. A less significant number-of-monolayers effect on the friction was observed for MXenes than for other studied 2D materials. In addition, the measured COFs did not depend on the applied normal forces (0-2 μ N) at contacts. These results reveal the potential of MXenes as excellent lubricants at the nanoscale for homoand heterostructured 2D materials.

2. Experimental Section

2.1. Sample Preparation

2.1.1. Synthesis of Graphene and Preparation of Graphene Samples on Si Substrates

Large-area monolayer graphene was grown by chemical vapor deposition (CVD) method on 25 µm thick copper foils (Alfa Aesar, CAS: 7440-50-8, LOT No. P17D009). Briefly, hydrogen and methane were fed into the reactor flow over the piece of copper foil, where methane was decomposed to carbon radicals at the Cu surface and then formed monolayer graphene. Then a thin layer of polymethyl methacrylate (PMMA) (4000 rpm for 30 s) was spin-coated on a Cu foil

with graphene on top and cured at 150 °C for 5 min. The foil was then etched away in Cu etchant (Sigma Aldrich, 667528) for 2 h. The monolayer graphene/PMMA sample was obtained by cleaning in deionized water. For bilayer graphene sample, monolayer graphene/PMMA was transferred to another freshly synthesized graphene on Cu foil followed by Cu etching. The tri- to five- layer graphene samples were prepared by repeating this procedure. Finally, the graphene and PMMA composite samples were transferred onto target Si (111)/SiO₂ substrates, pre-cleaned by bath sonication in acetone and hydrophilized in piranha solution, followed by thorough rinsing with deionized water. PMMA was removed by soaking in acetone solution and the residue of PMMA was removed by annealing at 400 °C in hydrogen and nitrogen mix for 2 h.

2.1.2. Synthesis of MoSe₂

MoSe₂ was synthesized on SiO₂ substrate by CVD method, using 700 mg of selenium (Se) (Sigma-Aldrich) and 15 mg of molybdenum oxide powder (Sigma-Aldrich) as the Se and Mo precursors, respectively. MoSe₂ was grown at 760 °C for 10 min under Ar/H₂ (15% H₂) flow.

2.1.3. Preparation of MXene Thin Films on Si Substrates and Spherical AFM Tips

Firstly, MAX phases were prepared using pressureless synthesis method. For Ti₂AlC MAX phase synthesis, titanium carbide (typically 2-micron size, 99.5%, Alfa Aesar), titanium (-325 mesh, 99%, Alfa Aesar), and aluminum (-325 mesh, 99.5%, Alfa Aesar) powders were ball-milled in a molar ratio of 0.85:1.15:1.05. The mixture was then heated at 1400 °C for 4 h under Ar flow in an alumina boat. For Ti₃AlC₂ MAX phase synthesis, titanium (-325 mesh, 99%, Alfa Aesar), aluminum (-325 mesh, 99.5%, Alfa Aesar), and graphite (-325 mesh, 99%, Alfa Aesar) powders were ball-milled in 3:1.1:1.88 molar ratio. Afterwards, the mixture was sintered at 1550 °C for 2 h in Ar flow in an alumina boat using a tube furnace (GSL-1800X -KS60-UL, MTI Corporation). The resulting ceramics were manually crushed into powders using pestle in a mortar. The selective etching of

Al from MAX phases (Ti₃AlC₂ and Ti₂AlC) to MXenes (Ti₃C₂T_x and Ti₂CT_x) procedure is as follows. Firstly, 0.3 g of MAX phase (-325 mesh, particle size \leq 45 µm) was slowly added to the etchant prepared by dissolving 0.3 g LiF in 3 mL 9 M HCl in a 50 mL plastic centrifuge tube. Then the mix was stirred for 36 h at 35 °C, followed by repeated washing with deionized water and centrifugation until the pH of supernatant reached 5.5-6.0. After 5 min handshaking and 1 h centrifugation at 3500 rpm, the obtained supernatant was used as MXene aqueous colloidal solution. Our original interfacial film deposition method described before [11, 16] was used to coat MXene thin films on SiO₂ substrates. At first, 50–300 μL of MXene colloidal solution was mixed in 50 mL DI water together with 3-6 mL toluene, and stirred for 15 min. Then the dispersion was poured directly into a beaker filled with 400 mL DI water and a few pieces of pre-cleaned Si substrates and spherical AFM tips placed at the bottom. After ~20 min standing still, when MXene films were self-assembled at the interface between water and toluene, the pieces of Si substrates or spherical AFM tips were slowly lifted up from the solution through the interface to catch the interfacial MXene films. Finally, the samples were dried in Ar flow at room temperature to avoid oxidation.

2.2. Characterization of Materials

2.2.1. Raman Spectroscopy

Raman spectroscopy was conducted on graphene, MoSe₂, Ti_2CT_x , and $Ti_3C_2T_x$ MXenes using Renishaw InVia confocal Raman microspectrometer with 532 nm laser, $20 \times$ objective, and 1200 l mm⁻¹ grating. Each spectrum was acquired over 10 s per accumulation at 10 % laser power and averaged over 3 accumulations.

2.2.2. X-Ray Diffraction (XRD) and Determination of the Number of Monolayers in MXene Films

XRD experiments were conducted on Ti_2CT_x and $Ti_3C_2T_x$ MXenes using (PANalytical, Philips MPD) with Cu K < α > radiation (λ =1.5406 Å) at U = 45 kV, I = 40 mA.

The number of monolayers in each sample was calculated by dividing the coating thickness (measured separately by AFM, see below) with a known d-spacing of a material.

2.2.3. X-Ray Photoelectron Spectroscopy (XPS)

XPS was recorded from Ti₂CT_x and Ti₃C₂T_x MXenes deposited on Si wafers using a KRATOS AXIS 165 X-Ray photoelectron spectrometer with a monochromatic Al X-Ray source. Charge neutralization was applied for the measurement. No sputtering was used.

2.2.4. Scanning Electron Microscopy (SEM)

SEM images were taken using Helios NanoLab 600 (FEI, Hillsboro, OR) with secondary electrons. The accelerating voltage was 5 kV, beam current 0.17 nA, and working distance 5 mm.

2.2.5. Roughness Measurements

Bare and Coated Tip: Tapping mode AFM scanning of the AFM spherical probes was conducted using Innova AFM (Bruker, Satan Barbara, CA) before and after the application of Ti₂CT_x or Ti₃C₂T_x MXene coating using a 3 nm radius AFM tip.

Substrate: AFM scans in tapping mode were performed on graphene, MoSe₂, Ti₂CT_x, or Ti₃C₂T_x MXene coated on Si substrates right before conducting friction measurements. The coating and substrate thickness and roughness were calculated from the line scans.

2.2.6. Friction Measurements

AFM was used for friction measurements on graphene, MoSe₂, Ti_2CT_x , and $Ti_3C_2T_x$ in lateral force mode with bare, Ti_2CT_x or $Ti_3C_2T_x$ MXene coated spherical SiO₂ tip (ACTG-TL, Appnano, Inc.). The spherical probe radius was 2.5 μ m, roughness 180 pm, and the cantilever stiffness \sim 33 N/m. The scan rate was 10 nm/s, and the scan distance 15 nm. In a typical friction experiment,

a specified normal force is applied, and the probe moves back and forth against the substrate surface to obtain the lateral deflection *versus* scan distance response (*i.e.*, trace and retrace curves). Six friction measurements with 2 nm spacing between the traces were performed on each flake. The value of lateral force is extracted from the lateral deflection changes originating from the twist of the cantilever of AFM tip. The method to convert the lateral deflection to lateral force and the procedure for calculating the lateral deflection signal conversion coefficient value are described in the Supplementary Information Note 1. The friction force was then obtained from the average of the maximal and minimal lateral forces in trace and retrace curves, respectively. All friction measurements were performed at room temperature and relative humility of 25%, measured with Protmex Digital Temperature Humidity Meter. To minimize MXene degradation, all MXene samples were measured within no more than 12 h from their preparation and drying, similar to the procedure used before [46].

Two series of friction measurements were conducted. In first series, we focus on the effect of normal force on COF of different 2D material interfaces. The tips are bare SiO₂, Ti₂CT_x, and Ti₃C₂T_x. The substrate materials are monolayer graphene, MoSe₂, Ti₂CT_x, and Ti₃C₂T_x deposited on SiO₂ surface. The normal forces were 0, 0.4, 0.8, 1.2, 1.6, and 2 µN. The monolayer substrate materials were characterized prior to the friction experiments using the methods mentioned above. With each normal force, six measurements were performed for every pair of interfaces to obtain the friction force with the scanning distance of 15 nm per measurement. The COFs were calculated from the applied normal force and the measured friction force.

In the second series of experiments, friction between SiO₂, Ti₂CT_x, Ti₃C₂T_x (tip materials), and 1 to 5 monolayers or bulk (>20 layers) graphene, MoSe₂, Ti₂CT_x, and Ti₃C₂T_x (substrate materials) was studied. The number of monolayers for substrate materials was determined prior to the friction

experiments as mentioned above. For each coating with the known number of monolayers of substrate material, six measurements were performed for each interface.

3. Results and Discussion

3.1. Materials Characterization

Raman spectra of graphene, MoSe₂, Ti₂CT_x, and Ti₃C₂T_x MXenes, confirming the identity of these materials, are shown in Fig. 1. Our graphene sample has characteristic Raman peaks at 1580 (G band) and 2700 cm⁻¹ (2D band) [47]. Monolayer graphene has a sharp 2D peak, which transforms to broader bands as the number of monolayers increases. The (I_G/I_{2D}) intensity ratio increases with the increased number of monolayers, and ranges from 0.3 to 3 [48] for 1-5 monolayer graphene. For more than 5 monolayers, the Raman spectrum becomes hardly distinguishable from that of bulk graphite [49]. Therefore, the bulk graphene with 21 monolayers was characterized by AFM (details could be found in Section 3.2). MoSe₂ shows characteristic Raman peaks between 200 and 360 cm⁻¹ [50]. Ti₂CT_x MXene shows characteristic Raman peaks at 200, 300, 374, 409, and 608 cm⁻¹. Ti₃C₂T_x MXene shows peaks at 206, 270, 374, 605, and 718 cm⁻¹ [46].

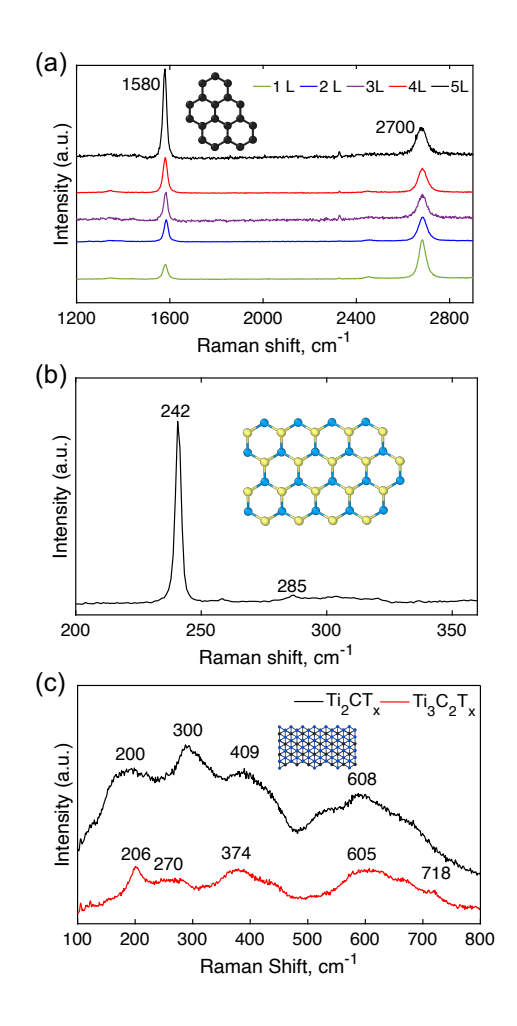


Fig. 1. Raman spectra for (a) 1-5 layers graphene, (b) monolayer MoSe₂, (c) Ti_2CT_x and $Ti_3C_2T_x$ flakes.

The d-spacing values for Ti₂CT_x and Ti₃C₂T_x are 1.36 nm and 1.48 nm, respectively, as calculated from XRD (Supplementary Information Fig. S1) using Bragg's law. The d-spacing for graphene stacks was assumed to be 0.37 nm [51]. Survey and high resolution XPS for Ti₂CT_x MXene are shown in Fig. S2a. For Ti₂CT_x MXene, peaks at 285.1 eV 459.6 eV 531.1 eV and 685.6 eV are attributed to C 1s, Ti 2p, O 1s and F 1s, respectively. F- and O-containing functional groups are introduced during the etching and delamination process. High-resolution spectrum of C 1s could be deconvoluted into four peaks at 282.2 eV, 283.2 eV, 284.9 eV and 286.4 eV, corresponding to C-Ti-(O/OH/F), COO, C-C, and C-OH, respectively. High-resolution spectrum of O 1s has peaks

at 529.3 eV, 529.9 eV, 531.2 eV, 532.0 and 533.8 eV, corresponding to Ti-O-C, TiO₂, Ti-C-O_x, Ti-C-OH_x, and H₂O. High-resolution spectrum of Ti 2p could be deconvoluted into eight peaks at 454.8 eV, 460.7 eV, 455.5 eV, 461.4 eV, 456.5 eV, 462.2 eV, 459.5 eV and 465.9 eV, which correspond to Ti-C (Ti₂P₃), Ti-C (Ti₂P₁), Ti(II) (Ti₂P₃), Ti(II) (Ti₂P₁), Ti(III) (Ti₂P₃), Ti(III) (Ti

3.2. Probe Coating and Substrate Material Profiles

Friction forces at SiO₂/graphene, SiO₂/MoSe₂, SiO₂/MXene, MXene/graphene, MXene/MoSe₂, and MXene/MXene interfaces were measured using a bare SiO₂ spherical probe or the probes coated with Ti₂CT_x or Ti₃C₂T_x MXene, respectively, as illustrated in Fig. 2a. SEM images of SiO₂ AFM probes before and after coating with MXenes are shown in Fig. 2b.

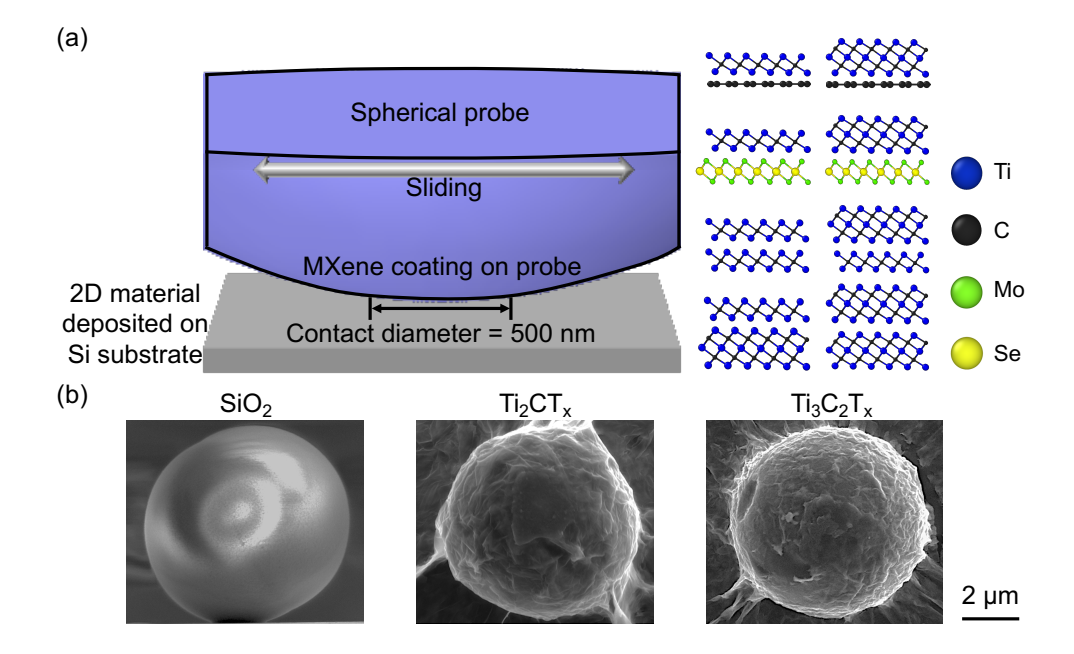


Fig. 2. (a) Schematics of AFM experiment for friction force measurements. (b) SEM images of bare SiO₂ spherical probe and MXene (Ti₃C₂T_x or Ti₂CT_x) coated SiO₂ spherical probes.

Line scans over the surface of bare SiO_2 and $MXene~(Ti_2CT_x~or~Ti_3C_2T_x)$ coated AFM probes are shown in Fig. 3a and b. The surface height profiles of $Ti_2CT_x~or~Ti_3C_2T_x~MXene~coating~layer$ (Fig. 3c) were obtained by image subtraction of the surface of bare SiO_2 probe from that of the MXene coated probe. From the line scans, the average coating thickness is $4.05~nm~for~Ti_2CT_x~and~4.41~nm~for~Ti_3C_2T_x~(Fig. 3d)$, meaning that three MXene monolayers were coated on these probes. The RMS roughness was $0.52~nm~for~Ti_2CT_x~and~0.28~nm~for~Ti_3C_2T_x~MXene$. The projected contact area during friction measurements was $\sim 500~nm \times 500~nm$.

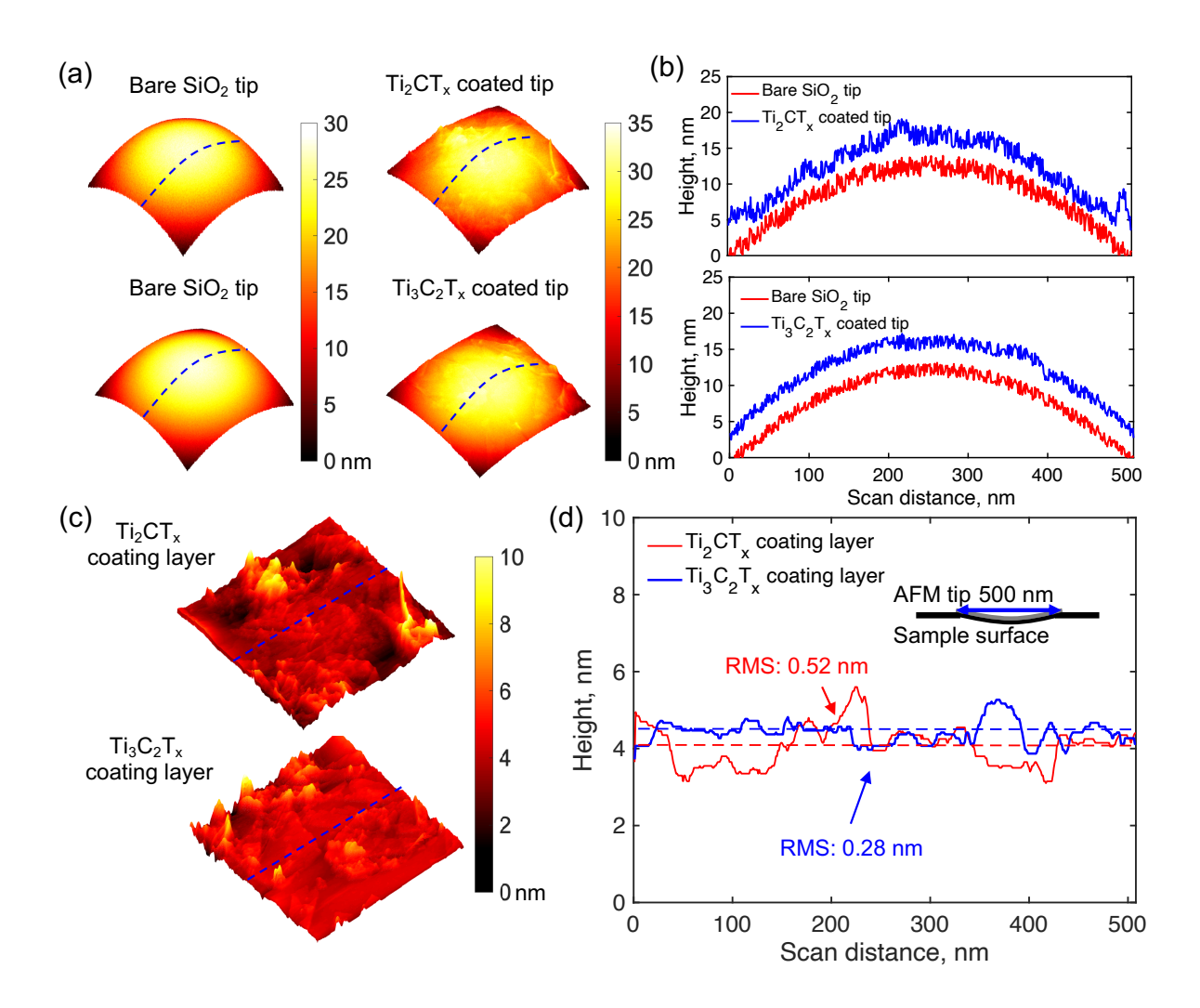


Fig. 3. (a) AFM maps of bare SiO₂, Ti₂CT_x or Ti₃C₂T_x MXene coated probes, (b) height profiles along the blue lines in (a), (c) morphology of Ti₂CT_x or Ti₃C₂T_x MXene coating layer, (d) height profiles along the blue lines in (c).

To obtain the number of monolayers and roughness of substrate materials, AFM scanning was conducted immediately before friction measurements. The typical AFM images for the monolayer graphene, MoSe₂, Ti₂CT_x, and Ti₃C₂T_x are shown in Fig. 4a. From the height versus scan distance curves (Fig. 4b), the thickness of graphene, MoSe₂, Ti₂CT_x, and Ti₃C₂T_x coatings is 0.35 nm, 1.01 nm, 1.32 nm, and 1.43 nm, respectively. The number of MXene monolayers was calculated by dividing the thickness of the coating with the d-spacing for Ti₂CT_x (1.36 nm) or Ti₃C₂T_x (1.48 nm), respectively. Using this method, we determined that our coatings were either 1-5 monolayers or nearly bulk Ti₂CT_x (24 layers) and Ti₃C₂T_x (25 layers). 1-5 monolayers and bulk MoSe₂ (18 layers) were determined by counting the number of MoSe₂ edges as shown in Fig. 4a and Fig. S3, using the same method as discussed in [53]. For 1-5 monolayers graphene, the number of monolayers was determined from Raman spectrum. Nearly bulk graphene coating (21 layers) was also confirmed by dividing the thickness of the coating with d-spacing value of graphite (0.35 nm). Surface roughness for graphene, MoSe₂, Ti₂CT_x, and Ti₃C₂T_x was also determined from the line scans. The typical RMS roughness values for the monolayer graphene, MoSe₂, Ti₂CT_x, and Ti₃C₂T_x were 94, 51, 67, and 60 pm, respectively, as shown in Fig. 4b.

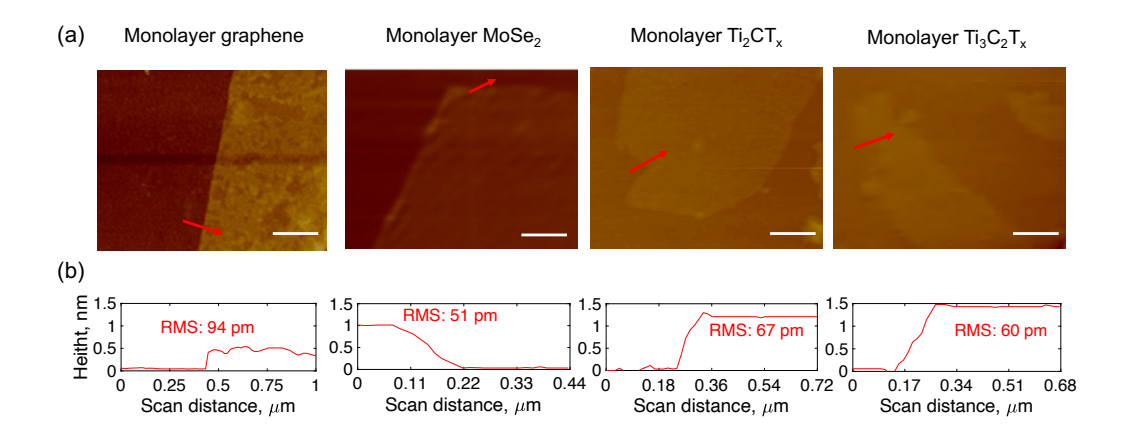


Fig. 4. (a) AFM images of 2D material films, and (b) line scans (along the red arrows in (a)) for monolayer graphene, MoSe₂, Ti₂CT_x, and Ti₃C₂T_x. Scale bars are 1 μm.

3.3. Friction Behavior of 2D Materials

3.3.1. Effect of Varying Normal Force on COFs

To investigate the effect of applied normal force on the COF, 6 different normal force values ranging from 0 μN to 2 μN were used in friction measurements. To check stability of the coating, first, friction measurements over 30 nm distance were performed under 2 μN normal force with Ti₂CT_x coated spherical tip on the same spot of the monolayer Ti₂CT_x. Lateral force *versus* scan distance curves and friction forces in Fig. S4 show no significant variations after 1080 scans. Thus friction between Ti₂CT_x and Ti₂CT_x didn't change after 1080 scans signifying stability of the MXenes for wear resistant contacts. The lateral force *versus* scan distance curves for friction measurements on the monolayer graphene, monolayer MoSe₂, monolayer Ti₂CT_x, and monolayer Ti₃C₂T_x using bare SiO₂ tip and MXene coated tips under 0, 0.4, 0.8, 1.2, 1.6, and 2 μN are shown in Fig. S5. The relatively flat trace and retrace curves reflect the low RMS roughness of the substrate materials. Friction forces (Table S1) were determined as the mean value of the maximum force in the trace portion of the loop and the minimum force in the retrace portion (dashed lines), following the method described in reference [32]. In addition, as shown by lateral force *versus*

scan distance curves in Fig. S5, lateral forces of each pair increased from the lowest lateral force (denoted by the bottom dash line) to the highest lateral force (denoted by the top dash line) after ~ 3 nm. Therefore, there won't be any scan distance effect on friction when the scan distance is higher than 3 nm. From the friction *versus* normal force graphs (Fig. 5), the friction force increased linearly with the increasing normal force for all contact pairs. The linear relationship between the friction force and the normal load is similar to that of the typical macroscopic friction law [54]. Moreover, a non-zero residual friction force is present at zero applied normal force, indicating the effect of substrate and probe material interactions.

The force ratio definition of COF:

$$COF = \frac{F_f - F_0}{F_n} \tag{1}$$

was adopted in this research, where F_f is the friction force, F_n is the applied normal force and F_0 is the offset friction force when the applied load is zero.

Since COF is constant, as observed from the linear relationship between friction and normal forces in Fig. 5, an intermediate normal force, 0.91 μ N, was used to investigate the number-of-monolayer and the monolayer thickness effects on COF values.

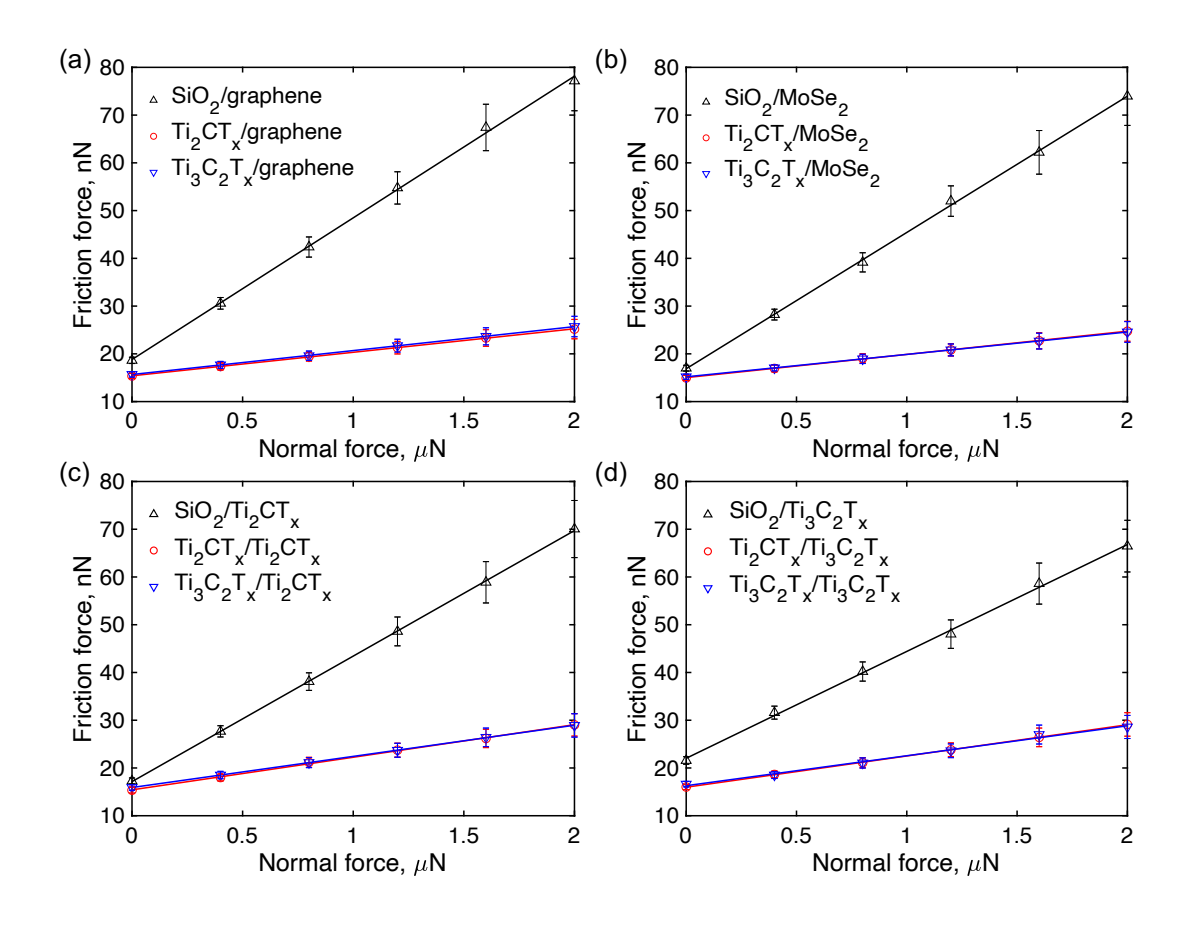


Fig. 5. Friction force *versus* normal force obtained from measurements on: (a) monolayer graphene, (b) monolayer MoSe₂, (c) monolayer Ti₂CT_x, and (d) monolayer Ti₃C₂T_x using bare SiO₂ and MXene coated probes as indicated in the corresponding graph legends. COF corresponds to the slope of these lines.

3.3.2. Interfacial COFs

The lateral force *versus* scan distance curves for friction measurements on 1-5 monolayers and bulk graphene, MoSe₂, Ti₂CT_x, and Ti₃C₂T_x using bare SiO₂ and MXene coated probes are shown in Fig. S6, and the calculated friction forces in Table S2. The measured friction forces under the applied normal forces 0 and 0.91 μ N were used to determine COF and F_0 listed in Table S1 and S2. The COF values with the corresponding standard deviations for all interfaces are listed in Table 1. The measurements showed that all 2D material interfaces achieved COF values lower than 0.01

when tested over 15 nm length. Among them, the lowest friction was found for $Ti_3C_2T_x/MoSe_2$ interface with a COF $(1.9\pm0.1)\times10^{-3}$. The highest friction was found for Ti_2CT_x/Ti_2CT_x interface with a COF $(6.8\pm0.2)\times10^{-3}$. In addition, both Ti_2CT_x and $Ti_3C_2T_x$ showed higher friction in sliding against themselves in comparison with sliding against graphene or $MoSe_2$. We suspect that the interactions between surface functional groups on MXene surfaces may lead to stronger interfacial MXene/MXene interactions manifested by higher friction.

Table 1. Measured COF values with standard deivations for all studied interfaces (bulk represents 21, 18, 24, and 25 layers for graphene, MoSe₂, Ti₂CT_x, and Ti₃C₂T_x, respectively)

Substrate Tip	# of monolayers	$COF \times 10^3$			
		Graphene	MoSe ₂	Ti ₂ CT _x	Ti ₃ C ₂ T _x
SiO ₂	1	30.1 ± 0.9	28.5 ± 0.8	26.2 ± 0.8	22.6 ± 0.7
	2	25.2 ± 0.5	22.3 ± 0.6	20.4 ± 0.5	19.5 ± 0.6
	3	23.6 ± 0.7	17.7 ± 0.4	15.3 ± 0.4	16.3 ± 0.5
	4	15.2 ± 0.5	14.6 ± 0.5	14.4 ± 0.3	15.3 ± 0.5
	5	11.4 ± 0.4	12.4 ± 0.4	13.4 ± 0.4	14.4 ± 0.5
	Bulk	10.9 ± 0.3	11.9 ± 0.4	13.2 ± 0.3	14.2 ± 0.4
Ti ₂ CT _x	1	5.3 ± 0.2	4.9 ± 0.2	6.8 ± 0.2	6.5 ± 0.3
	2	4.6 ± 0.1	4.2 ± 0.1	5.9 ± 0.2	5.7 ± 0.2
	3	3.9 ± 0.1	3.6 ± 0.1	5.2 ± 0.1	4.8 ± 0.1
	4	3.2 ± 0.1	2.9 ± 0.1	4.8 ± 0.1	4.5 ± 0.1
	5	2.6 ± 0.1	2.2 ± 0.1	4.4 ± 0.1	4.2 ± 0.1
	Bulk	2.5 ± 0.1	2.2 ± 0.2	4.4 ± 0.2	4.1 ± 0.1
Ti ₃ C ₂ T _x	1	5.1 ± 0.1	4.7 ± 0.2	6.5 ± 0.3	6.3 ± 0.3
	2	4.3 ± 0.2	4.0 ± 0.1	5.6 ± 0.2	5.4 ± 0.2
	3	3.7 ± 0.1	3.3 ± 0.2	4.9 ± 0.2	4.6 ± 0.2
	4	2.9 ± 0.1	2.7 ± 0.1	4.5 ± 0.1	4.2 ± 0.1
	5	2.3 ± 0.1	1.9 ± 0.1	4.2 ± 0.1	3.9 ± 0.1
	Bulk	2.3 ± 0.1	1.9 ± 0.1	4.1 ± 0.1	3.9 ± 0.1

The effect of the number of monolayers of a material on the measured interfacial COF is shown in Fig. 6. As the number of monolayers increases, the COF initially quickly drops until the number of MXene monolayers on the substrate reaches 3, after which the COF changes less dramatically. Similar 'reduction-to-steady' trend is known in literature for other materials [42]. It was reported that as the number of 2D monolayers increases, the increasing out-of-plane stiffness of the stack

reduces the elastic deformation at contact, which in turn reduces the "puckering" effect [42] as illustrated in Fig. 6d, hence, leading to a lower friction force.

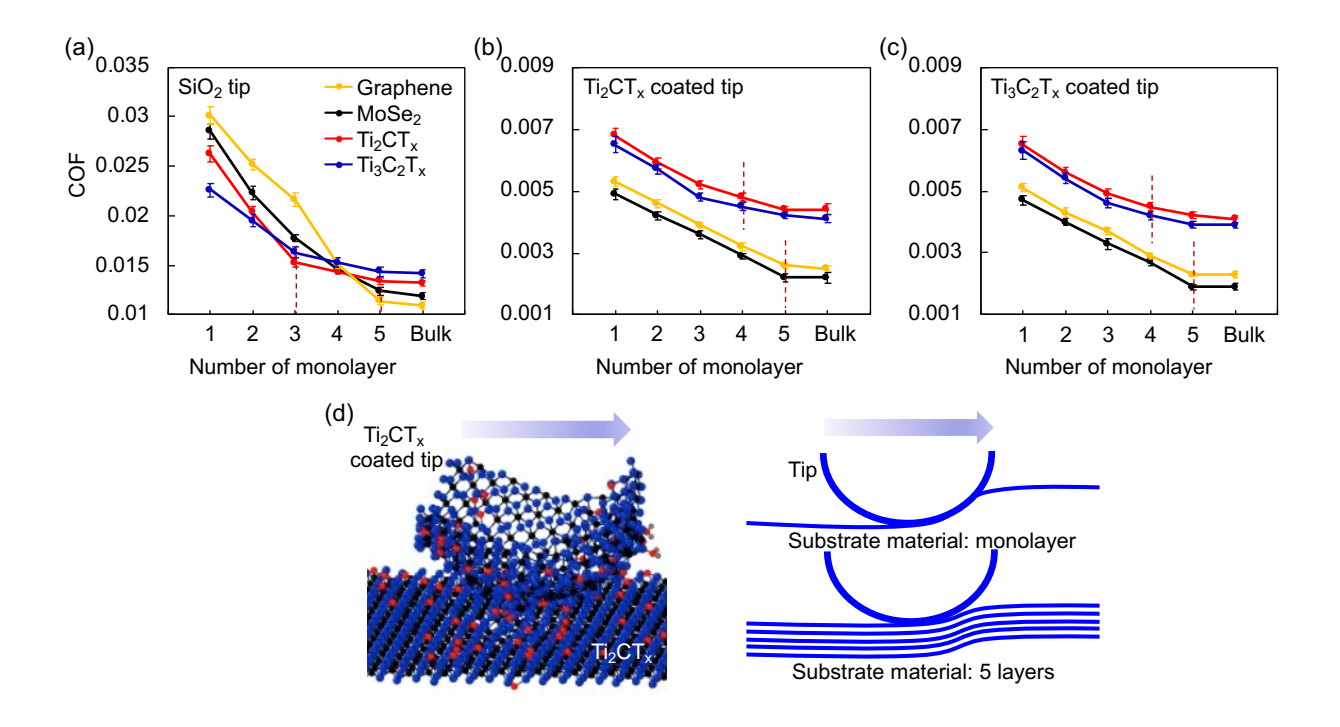


Fig. 6. COFs (with standard deviations) *versus* number of monolayers of graphene, MoSe₂, Ti₂CT_x, and Ti₃C₂T_x on a substrate, measured using (a) bare SiO₂ tip, (b) Ti₂CT_x coated, and (c) Ti₃C₂T_x coated tips (same graph legend applies to (a), (b), and (c)). Critical number of monolayers, at which the drop in COF with the number of monolayers ceased, is denoted by dashed lines. Bulk corresponds to 21, 18, 24, and 25 layers of graphene, MoSe₂, Ti₂CT_x, and Ti₃C₂T_x, respectively. (d) Schematic illustration of puckering effect as the thickness of a coating changes.

In addition, COFs measured with a bare SiO₂ tip decrease from graphene to MoSe₂, and to MXenes. This is mainly due to the increasing out-of-plane bending rigidity. The thickness for graphene, MoSe₂, Ti₂C, and Ti₃C₂ are 0.37 nm, 1.01 nm,1.36 nm and 1.48 nm respectively [24]. And the inplane stiffness are reported to be 335 N/m [55], 105 N/m [56], 135.53 N/m, and 214.85 N/m [57], respectively. Considering similar Poisson's ratio, the out-of-plane bending rigidity is lowest for

graphene, followed by MoSe₂, Ti₂C, and Ti₃C₂ MXenes. Lower out-of-plane bending rigidity introduced more out-of-plane deformation and tip-sample contact area during friction measurements, resulting in higher friction forces and COFs. Moreover, the measured COF values for MXene/monolayer MXene are higher than those for MXene/monolayer graphene and MXene/monolayer MoSe₂ interfaces. This may be due to hydrogen bonding mediated by the surface terminating groups (-O-, -OH, -F) between MXene layers. A similar effect of surface terminating groups on adhesion of Ti₃C₂T_x MXene was reported before [24, 58]. It should also be noted here that the surface defects and other terminating groups may also affect the friction of MXenes. However, these effects were not considered as dominant.

4. Conclusions and Outlook

In summary, we provide experimental data on the nanoscale friction bewtween MXenes and several other 2D materials measured using AFM. MXenes have demonstrated extremely low interfacial friction against themselves, graphene, and MoSe₂. The extremely low COFs (≤ 0.01) measured in this work at the nanometer scale (15 nm sliding distance) indicate a possible superlubric behavior when MXenes are in contact with other 2D materials at the nano- and possibly larger scales. All examined interfaces showed a gradual reduction of friction when the number of monolayers of a material has increased. This effect was prominent when the number of monolayers was 3 for interfaces invloving MXenes and 5 for the other 2D material interfaces. We suspect that this number-of-monolayer dependence of COF is most likely due to the nano-scale material deformations at the contact. When the total thickness of the stack of 2D material monolayers increases, its in-plane stiffness also increases, leading to less contact deformation and hence, to a reduced COF. Among the tested friction pairs, higher friction forces were measured for MXene/MXene contacts. To date, most studies of MXene friction were only performed with Ti-

based MXenes. Large structural diversity and compositional space of MXenes lend significant possibilities for optimization of MXene frictional and wear performance.

CRediT Authorship Contribution Statement

Yanxiao Li synthesized graphene, performed friction measurements and graphene characterization, analyzed data, and wrote the manuscript. Shuohan Huang synthesized MXene, performed MXene characterization, prepared MXene coatings using the interfacial film self-assembly technique, and wrote the manuscript. Congjie Wei wrote the manuscript. Dong Zhou synthesized MoSe₂, performed MoSe₂ characterization. Chenglin Wu, Vadym N. Mochalin, and Bo Li conceived and supervised the project, designed experiments, and revised the manuscript. All the authors reviewed, discussed and approved the results and conclusions of the paper.

Declaration of Competing Interest

The authors declare no competing financial interest.

Acknowledgments

Yanxiao Li, Shuohan Huang, Congjie Wei, Vadym N. Mochalin and Chenglin Wu gratefully acknowledge financial support of this work by the National Science Foundation through Grant no. CMMI-1930881. Yanxiao Li, Congjie Wei, and Chenglin Wu also would like to acknowledge financial support by the National Science Foundation through Grant no. CMMI-2045070. These authors also acknowledge help from Xiaoqing He from University of Missouri, Columbia. Dong Zhou and Bo Li acknowledge the Villanova University startup fund.

Appendix A. Supplementary data

References

[1] A. VahidMohammadi, J. Rosen, Y. Gogotsi, The world of two-dimensional carbides and nitrides (MXenes), Science 372 (2021) eabf1581.

- [2] B.C. Wyatt, A. Rosenkranz, B. Anasori, 2D MXenes: tunable mechanical and tribological properties, Adv. Mater. 33 (2021) 2007973.
- [3] M. Naguib, V.N. Mochalin, M.W. Barsoum, Y. Gogotsi, 25th anniversary article: MXenes: a new family of two-dimensional materials, Adv. Mater. 26 (2014) 992-1005.
- [4] X. Zhang, Z. Zhang, Z. Zhou, MXene-based materials for electrochemical energy storage, J. Energy Chem. 27 (2018) 73-85.
- [5] S. Bai, M. Yang, J. Jiang, X. He, J. Zou, Z. Xiong et al., Recent advances of MXenes as electrocatalysts for hydrogen evolution reaction, NPJ 2D Mater. Appl. 5 (2021) 1-15.
- [6] J.-C. Lei, X. Zhang, Z. Zhou, Recent advances in MXene: Preparation, properties, and applications, Front. Phys. 10 (2015) 276-286.
- [7] R. Khatun, M.A. Rahman, K.M. Hossain, M.Z. Hasan, M. Rasheduzzaman, S. Sarker, Physical properties of MAX phase Zr₂PbC under pressure: Investigation via DFT scheme, Physica B Condens. Matter 620 (2021) 413258.
- [8] Y. Lu, A. Yang, Y. Duan, M. Peng, Structural stability, electronic and optical properties of MAX-phase ternary nitrides β -TM₄AlN₃ (TM. = V, Nb, and Ta) using the first-principles explorations, Vacuum 193 (2021) 110529.
- [9] X. Jiang, A.V. Kuklin, A. Baev, Y. Ge, H. Ågren, H. Zhang et al., Two-dimensional MXenes: from morphological to optical, electric, and magnetic properties and applications, Phys. Rep. 848 (2020) 1-58.
- [10] M. Iqbal, J. Fatheema, Q. Noor, M. Rani, M. Mumtaz, R.-K. Zheng et al., Co-existence of magnetic phases in two-dimensional MXene, Mater. Today Chem. 16 (2020) 100271.
- [11] Y. Dong, S. Chertopalov, K. Maleski, B. Anasori, L. Hu, S. Bhattacharya et al., Saturable absorption in 2D Ti₃C₂ MXene thin films for passive photonic diodes, Adv. Mater. 30 (2018) 1705714.
- [12] J. Yi, J. Li, S. Huang, L. Hu, L. Miao, C. Zhao et al. Ti₂CT_x MXene-based all-optical modulator, InfoMat 2 (2020) 601-609.
- [13] J. Yi, L. Du, J. Li, L. Yang, L. Hu, S. Huang et al., Unleashing the potential of Ti₂CT_x MXene as a pulse modulator for mid-infrared fiber lasers, 2D Mater. 6 (2019) 045038.
- [14] S.J. Kim, H.-J. Koh, C.E. Ren, O. Kwon, K. Maleski, S.-Y. Cho et al., Metallic Ti₃C₂T_x MXene gas sensors with ultrahigh signal-to-noise ratio, ACS Nano 12 (2018) 986-993.
- [15] Y. Pei, X. Zhang, Z. Hui, J. Zhou, X. Huang, G. Sun et al., Ti₃C₂T_x MXene for Sensing Applications: Recent Progress, Design Principles, and Future Perspectives, ACS Nano 15 (2021) 3996-4017.
- [16] S. Chertopalov, V.N. Mochalin, Environment-sensitive photoresponse of spontaneously partially oxidized Ti₃C₂ MXene thin films, ACS Nano 12 (2018) 6109-6116.
- [17] Y. Dong, S.S.K. Mallineni, K. Maleski, H. Behlow, V.N. Mochalin, A.M. Rao et al., Metallic MXenes: A new family of materials for flexible triboelectric nanogenerators, Nano Energy 44 (2018) 103-110.
- [18] S. Zheng, H. Wang, P. Das, Y. Zhang, Y. Cao, J. Ma et al., Multitasking MXene inks enable high-performance printable microelectrochemical energy storage devices for all-flexible self-powered integrated systems, Adv. Mater. 33 (2021) 2005449.
- [19] X. Jia, B. Shen, L. Zhang, W. Zheng, Construction of compressible Polymer/MXene composite foams for high-performance absorption-dominated electromagnetic shielding with ultra-low reflectivity, Carbon 173 (2021) 932-940.

- [20] H. Liu, R. Fu, X. Su, B. Wu, H. Wang, Y. Xu et al., Electrical insulating MXene/PDMS/BN composite with enhanced thermal conductivity for electromagnetic shielding application, Compos. Commun. 23 (2021) 100593.
- [21] G. Li, N. Amer, H.A. Hafez, S. Huang, D. Turchinovich, V.N. Mochalin et al., Dynamical control over terahertz electromagnetic interference shielding with 2D Ti₃C₂T_y MXene by ultrafast optical pulses, Nano Lett. 20 (2019) 636-643.
- [22] A. Iqbal, P. Sambyal, C.M. Koo, 2D MXenes for electromagnetic shielding: a review, Adv. Funct. Mater. 30 (2020) 2000883.
- [23] A. Iqbal, J. Kwon, M.-K. Kim, C. Koo, MXenes for electromagnetic interference shielding: Experimental and theoretical perspectives, Mater. Today Adv. 9 (2021) 100124.
- [24] Y. Li, S. Huang, C. Wei, D. Zhou, B. Li, C. Wu et al., Adhesion between MXenes and other 2D materials, ACS Appl. Mater. Interfaces 13 (2021) 4682-4691.
- [25] M. Marian, G.C. Song, B. Wang, V.M. Fuenzalida, S. Krauß, B. Merle, S. Tremmel, S. Wartzack, J. Yu, A. Rosenkranz, Effective usage of 2D MXene nanosheets as solid lubricant—Influence of contact pressure and relative humidity, Appl. Surf. Sci. 531 (2020) 147311.
- [26] M. Marian, S. Tremmel, S. Wartzack, G. Song, B. Wang, J. Yu, A. Rosenkranz, MXene nanosheets as an emerging solid lubricant for machine elements—Towards increased energy efficiency and service life, Appl. Surf. Sci. 523 (2020) 146503.
- [27] A. Levitt, J. Zhang, G. Dion, Y. Gogotsi, J.M. Razal, MXene-based fibers, yarns, and fabrics for wearable energy storage devices, Adv. Funct. Mater. 30 (2020) 2000739.
- [28] Y. Lei, W. Zhao, Y. Zhang, Q. Jiang, J.H. He, A.J. Baeumner, O.S. Wolfbeis, Z.L. Wang, K.N. Salama, H.N. Alshareef, A MXene-based wearable biosensor system for high-performance in vitro perspiration analysis, Small 15 (2019) 1901190.
- [29] S. Huang, K. Mutyala, A. Sumant, V. Mochalin, Achieving superlubricity with 2D transition metal carbides (MXenes) and MXene/graphene coatings, Mater. Today Adv. 9 (2021) 100133.
- [30] A. Rosenkranz, P.G. Grützmacher, R. Espinoza, V.M. Fuenzalida, E. Blanco, N. Escalona et al., Multi-layer Ti₃C₂T_x-nanoparticles (MXenes) as solid lubricants–Role of surface terminations and intercalated water, Appl. Surf. Sci. 494 (2019) 13-21.
- [31] Y. Guan, M. Zhang, J. Qin, X. Ma, C. Li, J. Tang, Hydrophilicity-dependent distinct frictional behaviors of different modified MXene nanosheets, J. Phys. Chem. C 124 (2020) 13664-13671.
- [32] Y. Guo, X. Zhou, D. Wang, X. Xu, Q. Xu, Nanomechanical Properties of Ti₃C₂ MXene, Langmuir 35 (2019) 14481-14485.
- [33] X. Zhou, Y. Guo, D. Wang, Q. Xu, Nano friction and adhesion properties on Ti₃C₂ and Nb₂C MXene studied by AFM, Tribol. Int. 153 (2021) 106646.
- [34] D. Berman, A. Erdemir, A.V. Sumant, Graphene: a new emerging lubricant, Mater. Today 17 (2014) 31-42.
- [35] S. Zhang, T. Ma, A. Erdemir, Q. Li, Tribology of two-dimensional materials: From mechanisms to modulating strategies, Mater. Today 26 (2019) 67-86.
- [36] J.C. Spear, B.W. Ewers, J.D. Batteas, 2D-nanomaterials for controlling friction and wear at interfaces, Nano Today 10 (2015) 301-314.
- [37] M.R. Vazirisereshk, H. Ye, Z. Ye, A. Otero-de-la-Roza, M.-Q. Zhao, Z. Gao, A.C. Johnson, E.R. Johnson, R.W. Carpick, A. Martini, Origin of nanoscale friction contrast between supported graphene, MoS₂, and a graphene/MoS₂ heterostructure, Nano lett. 19 (2019) 5496-5505.
- [38] D.-H. Cho, L. Wang, J.-S. Kim, G.-H. Lee, E.S. Kim, S. Lee, S.Y. Lee, J. Hone, C. Lee, Effect of surface morphology on friction of graphene on various substrates, Nanoscale 5 (2013) 3063-3069.

- [39] D. Berman, A. Erdemir, A.V. Zinovev, A.V. Sumant, Nanoscale friction properties of graphene and graphene oxide, Diam. Relat. Mater. 54 (2015) 91-96.
- [40] Q. Li, C. Lee, R.W. Carpick, J. Hone, Substrate effect on thickness-dependent friction on graphene, Phys. Status Solidi B 247 (2010) 2909-2914.
- [41] X. Lin, H. Zhang, Z. Guo, T. Chang, Strain engineering of friction between graphene layers, Tribol. Int. 131 (2019) 686-693.
- [42] C. Lee, Q. Li, W. Kalb, X.-Z. Liu, H. Berger, R.W. Carpick et al., Frictional characteristics of atomically thin sheets, Science 328 (2010) 76-80.
- [43] V.N. Borysiuk, V.N. Mochalin, Y. Gogotsi, Bending rigidity of two-dimensional titanium carbide (MXene) nanoribbons: A molecular dynamics study, Comput. Mater. Sci. 143 (2018) 418-424.
- [44] S.I. Yengejeh, S.A. Kazemi, W. Wen, Y. Wang, Multiscale numerical simulation of in-plane mechanical properties of two-dimensional monolayers, RSC Adv. 11 (2021) 20232-20247.
- [45] A. Rodriguez, M. Jaman, O. Acikgoz, B. Wang, J. Yu, P. Grützmacher, A. Rosenkranz, M. Baykara, The Potential of Ti₃C₂T_x nano-sheets (MXenes) for nanoscale solid lubrication revealed by friction force microscopy, Appl. Surf. Sci. 535 (2021) 147664.
- [46] Y. Li, S. Huang, C. Wei, C. Wu, V.N. Mochalin, Adhesion of two-dimensional titanium carbides (MXenes) and graphene to silicon, Nat. Commun. 10 (2019) 1-8.
- [47] A. Ismach, C. Druzgalski, S. Penwell, A. Schwartzberg, M. Zheng, A. Javey et al., Direct chemical vapor deposition of graphene on dielectric surfaces, Nano Lett. 10 (2010) 1542-1548.
- [48] A. Gupta, G. Chen, P. Joshi, S. Tadigadapa, P. Eklund, Raman scattering from high-frequency phonons in supported n-graphene layer films, Nano Lett. 6 (2006) 2667-2673.
- [49] A.C. Ferrari, J.C. Meyer, V. Scardaci, C. Casiraghi, M. Lazzeri, F. Mauri, S. Piscanec, D. Jiang, K.S. Novoselov, S. Roth, Raman spectrum of graphene and graphene layers, Phys. Rev. Lett. 97 (2006) 187401.
- [50] D. Nam, J.-U. Lee, H. Cheong, Excitation energy dependent Raman spectrum of MoSe₂, Sci. Rep. 5 (2015) 1-6.
- [51] R. Siburian, D. Sari, J. Gultom, H. Sihotang, S. Raja, M. Supeno, Performance of graphite and graphene as electrodes in primary cell battery, J. Phys. Conf. Ser. 1116 (2018) 042034.
- [52] J. Halim, K.M. Cook, M. Naguib, P. Eklund, Y. Gogotsi, J. Rosen, M.W. Barsoum, X-ray photoelectron spectroscopy of select multi-layered transition metal carbides (MXenes), Appl. Surf. Sci. 362 (2016) 406-417.
- [53] A.V. Agrawal, R. Kumar, G. Yang, J. Bao, M. Kumar, M. Kumar, Enhanced adsorption sites in monolayer MoS₂ pyramid structures for highly sensitive and fast hydrogen sensor, Inter. J. Hydrog. Energy 45 (2020) 9268-9277.
- [54] Y. Mo, K.T. Turner, I. Szlufarska, Friction laws at the nanoscale, Nature 457 (2009) 1116-1119.
- [55] M. Topsakal, S. Cahangirov, S. Ciraci, The response of mechanical and electronic properties of graphane to the elastic strain, Appl. Phys. Lett. 96 (2010) 091912.
- [56] Y.-J. Zhang, R.-N. Wang, G.-Y. Dong, S.-F. Wang, G.-S. Fu, J.-L. Wang, Mechanical properties of 1 T-, 1 T'-, and 1 H-MX₂ monolayers and their 1 H/1 T'-MX₂ (M= Mo, W and X= S, Se, Te) heterostructures, AIP Adv. 9 (2019) 125208.
- [57] T. Hu, J. Yang, W. Li, X. Wang, C.M. Li, Quantifying the rigidity of 2D carbides (MXenes), Phys. Chem. Phys. 22 (2020) 2115-2121.
- [58] B. Tang, C. Tang, L. Chen, C. Xiao, A. Rosenkranz, L. Qian, Nanoscopic humidity-dependent adhesion behaviors of 2D materials, Appl. Surf. Sci. 572 (2022) 151394.